JCTC Journal of Chemical Theory and Computation

Article

pubs.acs.org/JCTC

Electronic Structure Study of Singlet Fission in Tetracene Derivatives

David Casanova*

IKERBASQUE, Basque Foundation for Science, 48011 Bilbao, Spain

Kimika Fakultatea, Euskal Herriko Unibertsitatea (UPV/EHU), P.K. 1072, 20080 Donostia, Spain

Donostia International Physics Center (DIPC), 20018 Donostia, Spain

Supporting Information

ABSTRACT: A detailed theoretical study of the singlet fission process in tetracene and two of its derivatives, that is 5,12-diphenyltetracene (DPT) and rubrene, is presented. This work aims to unravel the intricacies and the differences of their singlet fission mechanism by means of electronic structure calculations using molecular and cluster models and a variety of computational tools. Although the electronic structure at the molecular level is very similar for the three compounds, their different crystal packing has important consequences in their ability to produce two triplet states from a single exciton. The results obtained indicate that the lowest singlet is found to delocalize at least over seven molecules. Computed relative energies rule out the presence of charge transfer (CT) states as intermediates in a two-step mechanism in all cases. On the other hand, CT states do play a role as mediators, specially in tetracene. They decisively participate in the coupling between single and multiexcitonic states through second-order contributions. Finally, the present study pinpoints that the transition from the optically allowed exciton to the dark multiexciton state might be facilitated by intramolecular motion toward the lowest excited singlet geometry.

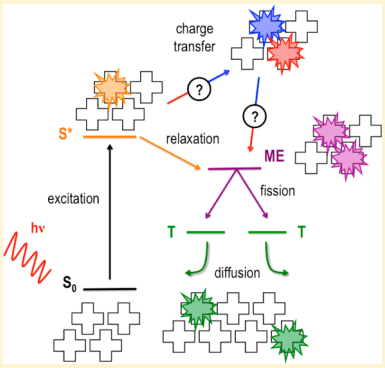

INTRODUCTION

The singlet fission (SF) mechanism is a special case of internal conversion between electronic states with the same spin multiplicity. In SF a single-exciton singlet state transitions into a state of multiexcitonic nature with the capacity to split in two coupled triplet excitations. This process has seen to be extremely fast, especially in organic molecular crystals with the appropriate conditions, where the nonadiabatic transit can occur in the ps and even subps time scale. The SF phenomenon was observed and described for the first time almost half a century ago in anthracene crystals.[1] Since then, SF has been invoked in other acene crystals such as tetracene,[2−5] pentacene,[6−9] and hexacene derivatives,[10] and also in carotenoids[11] and conjugated polymers.[12]

The interest toward the SF idea was strongly revitalized in 2004 with the work of Nozik and collaborators,[13] where SF was proposed as a possible electronic mechanism to increase the efficiency of photoelectric conversion. In the past few years, SF has become one of the most promising multiexciton generation mechanisms for solar energy conversion.[4,9,14−19] In theory, the SF process would allow the production of two excited electrons for each harvested photon and thus surpass the Shockley−Queisser theoretical limit of single junction solar cells.[20] But, despite all the theoretical[21−25] and practical[9,26−30] advances made in the field, some aspects and intricacies of the SF mechanism cannot be considered fully resolved, and there is yet a long and arduous pathway to go until SF can be effectively applied in real photovoltaic devices.

Because of the SF origins, acene-based materials have been the most paradigmatic compounds able to undergo SF. Among them, tetracene and pentacene have been largely scrutinized experimentally, which has resulted in great advances in the understanding of structural and electronic parameters controlling the SF efficiency. In the past few years, several works have looked at SF of substituted acenes. In particular, SF has been found to be favored in two chemical derivatives of tetracene, that is, 5,12-diphenyltetracene (DPT)[31] and rubrene.[17,32−35] Understanding of SF in these systems and the rationalization of their distinctive SF properties should help to bring the field one step closer to greater goals.

The present work aims to describe structural and electronic properties in relation to the SF capability of tetracene, DPT, and rubrene by using ab initio computational tools. First, I will revisit nuclear and electronic structure characteristics related to photophysical properties of the three molecular species in solution. These preliminary results will serve as a foundation for the subsequent investigation of the SF mechanism in the extended structures. I will analyze the localization degree of the single exciton. I will put special attention in understanding the role of charge transfer (CT) states in accessing the multiexcitonic state. I will decompose the coupling between initial (optical) and final (dark) states in direct and mediated interaction contributions by means of the first- and second-order perturbation theory, respectively. Finally, I will propose

Received: August 29, 2013

dx.doi.org/10.1021/ct4007635 | J. Chem. Theory Comput. XXXX, XXX, XXX−XXX

Table 1. Ground and Excited States Structural Parameters (depicted in Figure 1) of Tc, DPT, and the Two Forms of Rub Optimized in Solution[a]

	α		β		γ		δ	
	S_0	S_1	S_0	S_1	S_0	S_1	S_0	S_1
Tc	–	–	–	–	–	–	0.0	0.0
DPT	90.7	91.0	–	–	84.5	65.4	0.1	0.0
Rub-*flat*	95.1	94.4	29.1	34.3	78.3	71.2	0.0	0.0
Rub-*twist*	94.7	94.5	39.0	43.5	64.9	56.2	44.2	48.5

[a] α, β, and γ correspond to average values.

and explore an intramolecular nuclear motion as a possible catalyst of SF in the studied materials.

NOMENCLATURE

The singlet fission concept is a pivotal element of this manuscript. Unfortunately, another important term used in the text, that is, spin flip, commonly uses the same abbreviation (SF). Despite this coincidence, the conceptual frame of the text is clear enough to avoid any potential confusion. Thus, the same acronym will be used for both terms. The names of the studied compounds will be abbreviated as Tc (tetracene), DPT (5,12-diphenyltetracene), and Rub (rubrene). Uppercase boldface symbols will indicate adiabatic electronic states, while italic uppercase characters will be used for configuration state functions (CSFs) also referred here as diabatic states.

COMPUTATIONAL DETAILS

Molecular geometries of Tc, DPT, and Rub in solution have been optimized with the B3LYP functional. Solvation effects have been introduced by means of the SM8 model.[36] For the sake of comparison to the available experimental data, computational simulations of Tc and DPT have been done in chloroform solution, while Rub was computed in toluene. Comparison between Rub geometries optimized in chloroform and toluene did not present major differences. Vibrational frequencies and electronic transitions in solution have been also computed with B3LYP. Comparison of vertical and adiabatic energies to other density functionals can be found in the Supporting Information. Time-dependent density functional theory (TDDFT)[37,38] calculations of single electronic excitations in molecular clusters have been done with the ωB97X-D[39] long-range-corrected (LRC) functional and with the SBKJC effective core potential and basis set.[40] See Figure S1 of the Supporting Information for a detailed description of the cluster models.

Electronic structure calculations of the dimer models have been done within the restricted active space configuration interaction (RASCI) formalism.[41−43] Electronic wave functions were built from a high spin ROHF quintet determinant as the reference configuration, with the RAS2 subspace including the four singly occupied orbitals and RAS1 (RAS3) subspace corresponding to the fully occupied (virtual) orbital space. The final computed states were obtained by means of electronic excitations with two simultaneous promotions of α-electrons into β-orbitals and with the hole and particle truncation in the CI expansion (RAS-2SF). Excitation energies to CT diabatic states in dimer models have been also calculated within the constrained density functional theory (CDFT) approach[44] and the ωB97X-D functional.

Unless indicated, all calculations have been carried out with the 6-31G* basis set and the Q-Chem package.[45]

DISCUSSION

A. Structural and Optical Properties in Solution. The optimized ground state molecular structure of Tc is perfectly planar (δ = 0° in Table 1, Figure 1) and belongs to the D_{2h}

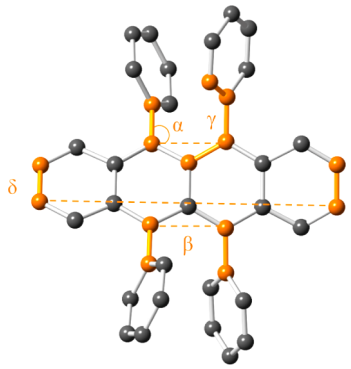

Figure 1. Description of the structural parameters in Table 1.

symmetry. Similarly, the tetracene carbon backbone in DPT is virtually planar with the side phenyl rings being almost perpendicular to the main molecular plane ($\alpha \sim 91°$ and $\gamma \sim 85°$). On the other hand, optimization of Rub converges into two stable geometries, corresponding to planar and twisted forms of the tetracene core (Figure 2). In the planar form (Rub-*flat*), the four fused rings lie almost perfectly on the same plane ($\delta \sim 0°$). The tiny departure from perfect planarity is related to the disposition of the phenyl rings. The side rings are almost perpendicular to the inner plane ($\alpha \sim 95°$), with the pairs of phenyls in trans located above and below the main plane ($\beta \sim 29°$). In the twisted form (Rub-*twist*), the torsion of the tetracene unit alleviates the strong steric hindrance between adjacent phenyl rings, inducing larger separation between phenyls ($\beta \sim 39°$). As a result, Rub-*twist* is energetically favored against the planar geometry by 3.6 kcal/mol. The computed torsion angle between the outermost carbon atoms in Rub-*twist* (δ = 44.2°) is very close to the 42° molecular torsion computed in gas phase.[46] On the other hand, the twisted form is unstable for both Tc and DPT molecules, which confirms the hypothesis that the phenyl−phenyl steric interactions are responsible for the twist of the molecule.

Vibrational frequency analysis of the structures confirms that they are all true potential energy minima. The computed symmetric CC stretching bond frequencies in the 1200−1500 cm^{-1} region (Table S1, Supporting Information) of the tetracene core are in very good agreement with the experimental measure of the strong vibrational progression in the absorption spectra associated to ring breathing modes, with an effective spacing of ~1400 cm^{-1} in the absorption spectra of

dx.doi.org/10.1021/ct4007635 | J. Chem. Theory Comput. XXXX, XXX, XXX−XXX

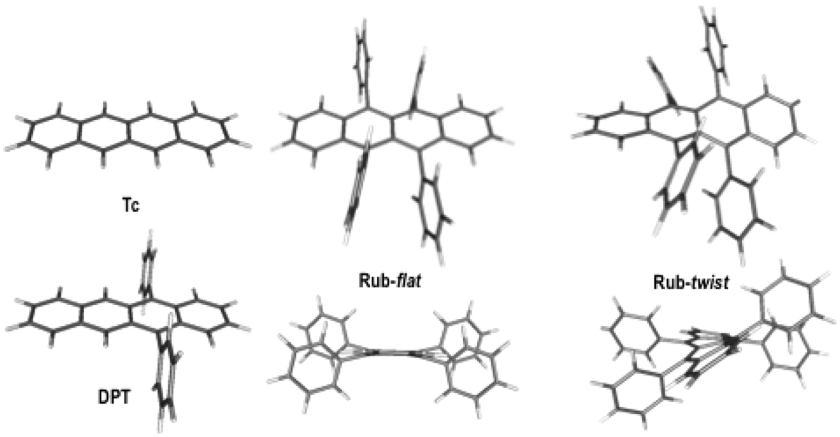

Figure 2. Ground state optimized geometries of Tc, DPT, and the two forms of Rub.

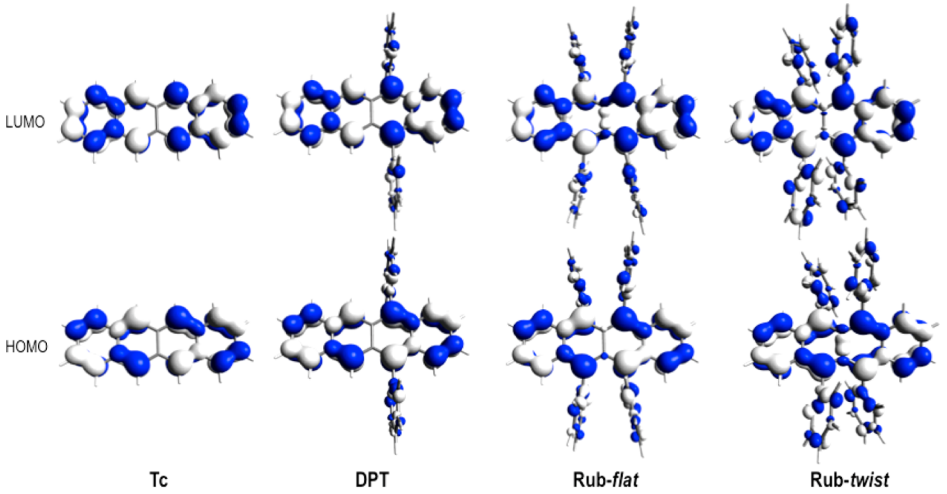

Figure 3. Isodensity representation of HOMO (bottom) and LUMO (top) of Tc, DPT, Rub-*flat*, and Rub-*twist*.

Tc and DPT in solution, and a little bit smaller in Rub (∼1300 cm^{-1}) due to its twisted form.[31,34,47]

The electronic structure of all tetracene-based molecules at the frontier between occupied and virtual orbitals is very much alike (Figure 3). The Tc HOMO and LUMO correspond to the a_u (π) and b_{2g} (π^*) orbitals, respectively. The frontier orbitals in DPT and Rub are also mainly located at the tetracene core and only incorporate small contributions from the side rings. Although there is an important loss of planarity in Rub-*twist*, the π-conjugation of the HOMO and LUMO is well preserved. The substitution phenyls in DPT and Rub act as an effective extension of the electronic conjugation; as a consequence, the HOMO−LUMO energy difference decreases with the number of side phenyl rings. The torsion of the carbon backbone in Rub-*twist* has a large impact on the occupied π-orbital, which is considerably destabilized with respect to the LUMO, reducing the orbital energy gap.

The electronic structure of the lowest excited singlet and triplet states mainly correspond to a single electron excitation between the two frontier orbitals. As a result, optimized geometries of the three studied molecules in the S_1 state show a systematic alternating increase and decrease in the CC bond distances within the tetracene backbone as depicted in Figure 4. The S_0 to S_1 distortion roughly corresponds to a combination of the breathing modes responsible for the vibrational progression in the absorption spectra. The molecular planarity

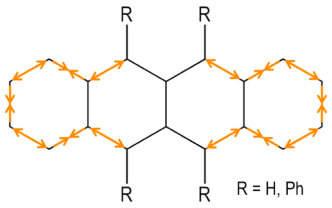

Figure 4. Molecular distortion of the tetracene backbone corresponding to the relaxation of the S_1 from the ground state geometry.

is preserved in all cases, only that the twisted form of Rub δ increases with respect to the ground state angle (∼ 4°). The side rings in DPT and Rub are further separated and twisted with respect to the tetracene plane, i.e., larger β and smaller γ angles.

Computed transitions are in very good agreement with the experimental values of absorption and emission maxima and the adiabatic excitation energies in solution (Table 2). Transition energies decrease with increasing the substitution degree, while vertical oscillator strengths systematically increase, consistent with an effective increase in the π-conjugation. The twisted form of Rub presents smaller energy gaps with respect to Rub-*flat*, as predicted by the larger relative destabilization of the HOMO in Rub-*twist*. In addition to the *flat*/*twist* ground state relative stability, comparison between computed and measured

dx.doi.org/10.1021/ct4007635 | J. Chem. Theory Comput. XXXX, XXX, XXX−XXX

Table 2. Vertical Transition to the Lowest Triplet $E(T_1)$, and Computed and Experimental[47] Absorption, Emission and Adiabatic ($E_{0\text{-}0}$) Excitation Energies for Tc, DPT, Rub-*flat*, and Rub-*twist* in solution[a]

		absorption			emission		E_{0-0}	
	$E(T_1)$	f	calc.	expt.[b]	calc.	expt.[c]	calc.	expt.
Tc	1.44	0.088	2.74	2.61	2.50	2.59	2.62	2.60
DPT	1.40	0.162	2.66	2.51	2.37	2.47	2.52	2.49
Rub-*flat*	1.30	0.228	2.54		2.27		2.41	
Rub-*twist*	1.25	0.259	2.39	2.36	2.09	2.23	2.24	2.29

[b]Absorption maxima. [c]Emission maxima. [a]Oscillator strengths f correspond to the vertical excitations at the ground state geometries. All energies are in eV.

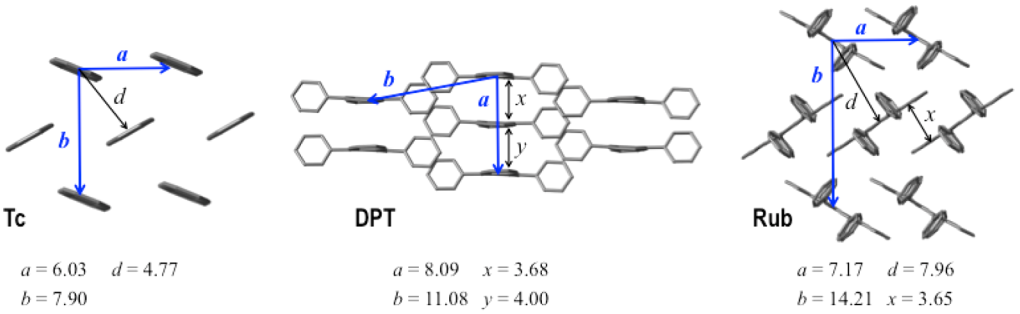

Figure 5. Crystal structures of Tc (left), DPT (center), and Rub (right) with the a and b lattice parameters and other relevant distances discussed in the text. All values are in Å. x and y distances in DPT correspond to separation between tetracene planes of staggered and eclipsed dimers, respectively.

vertical absorption energies points to Rub-*twist* as being the predominant form in solution.

Vertical energies in Table 2 suggest that the necessary thermodynamic condition for the split of the singlet exciton into two triplets is not perfectly met, i.e., $2E(T_1) - E(S_1) \sim 0.1$ eV, coherent with a higher-energy multiexcitonic state in Tc.[3,7,48] The energy gap decreases with the phenyl substitution on the tetracene backbone, with $2E(T_1) - E(S_1) = 140$, 137, 107, and 57 meV for Tc, DPT, Rub-*twist*, and Rub-*flat*, respectively.

B. Extended Structures of Tc, DPT and Rub. The crystal structure of Tc[49,50] presents a herringbone motif (Figure 5). Long molecular axes are aligned perpendicular to the *ab* plane, while the short axis of neighbor molecules form an angle of ~51°. The significant short-axis displacement and intermolecular separation frustrate the interactions along a and b directions, respectively. As a consequence, the main electronic couplings occur in the diagonal direction (d). The relative orientation between adjacent Tc molecules along d leads to oblique π-interactions between chromophores.

Steric hindrance due to the side bulky phenyl rings in DPT and Rub gives rise to important differences in their crystal packing with respect to Tc. Molecules in DPT crystals are stacked along the crystal's a-axis (Figure 5),[31,51] with all tetracene cores arranged virtually coplanar. The long axes of consecutive stacked molecules are a bit displaced, alternating between eclipsed and staggered conformations.

In contrast to the most stable (twisted) geometry in solution, the tetracene backbone in crystal Rub adopts a highly planar form.[52] The crystal packing, like Tc, presents a herringbone motif, but in Rub the long molecular axes lies in the *ab* plane. As a consequence, the molecular axes of adjacent monomers form ~61°, far from the parallel disposition in Tc. A crucial feature of Rub's extended structure is the π-stacking along the a-axis, with 3.65 Å separation between tetracene cores (x in Figure 5) and no displacement along the shorter axes. In spite of the large displacement of neighbor molecules in the long molecular axis (~6.13 Å), experimental[53] and computational[54] studies of the charge transport properties in Rub indicate that interactions in the a direction retain a large fraction of the maximum perfect cofacial stacking and that the electronic couplings are much stronger than in the diagonal direction (Figure 5).

Optical Exciton Characterization. The delocalization character of the optically excited state in the extended structures, that is, the number of molecules involved in the initial photoexcitation, constitutes an important property in order to understand the posterior nonadiabatic evolution of the system. Therefore, aiming to capture the nature and properties of the lowest excited singlet, I analyze the dependence of the S_0 to S_1 transition energy with the number of molecules n for the three chromophores with the frozen atomic structure in the crystal discussed above (Figure 6 and Table S3, Supporting Information). Computed energies of the molecular clusters have been linearly fitted to the invers of n (eq 1), which allows to extract an estimation of the transition in the crystal ($E_1(\infty)$). Excitation energies to S_1 seem to converge for clusters beyond seven molecules, with energies <0.05 eV over the $n \rightarrow \infty$ limit. Extrapolated energies are very close (0.04−0.10 eV larger) to the results of Zimmerman et al.[55] for Tc clusters with $n = 4$ and 10, who used a similar level of theory. Obtained energy profiles are in line with time-resolved spectroscopy measurements indicating that the optical exciton in Tc approximately delocalizes over 10 molecules.[56]

$$E_1(n) = E_1(\infty) + \frac{A}{n} \quad (1)$$

$E_1(\infty)$ for Tc, DPT, and Rub are, respectively, 2.98, 2.85, and 2.83 eV, which are systematically 0.6−0.7 eV higher than experimental values. This is the same overestimation obtained in the computation of transition energies in solution with ωB97X-D (Supporting Information). On the other hand, their

dx.doi.org/10.1021/ct4007635 | J. Chem. Theory Comput. XXXX, XXX, XXX−XXX

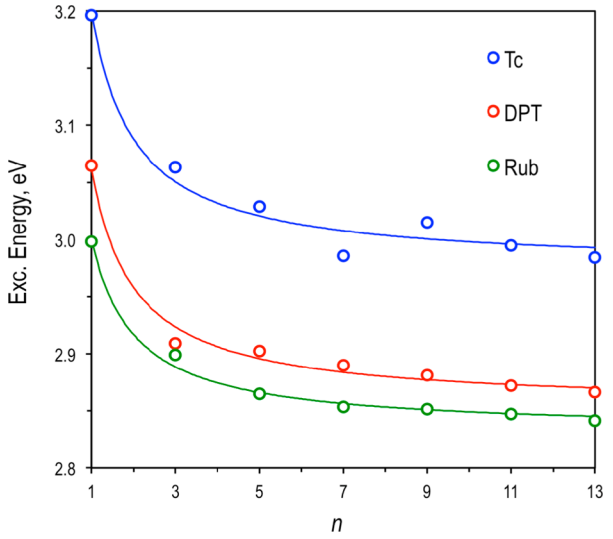

Figure 6. Excitation energies of Tc, DPT, and Rub clusters as a function of the cluster size (number of molecules).

relative differences are in very good agreement with experimental absorption spectra.[31,34] Therefore, the error in $E_1(\infty)$ can be simply attributed to the systematic overestimation of the excitation energy by ωB97X-D at the monomer level.

The A slope in eq 1 informs about the average increase (decrease) of the transition energy per molecule. Thus, it can be seen as a qualitative measure of the average strength of intermolecular coupling. The fitted values for the three compounds are 0.225, 0.208, and 0.169 eV/molecule, indicating a decrease in the intermolecular interaction along the Tc > DPT > Rub series.

As has been observed in some covalently linked organic dimers,[57,58] SF can take place through a two-step mechanism with a CT intermediate assisting the process by an electron transfer from S_0S_1 to the CT state and a subsequent back electron transfer form the CT state to the TT state. In order to explore the energetic accessibility of the two-step channel, and considering the estimated spatial extend of the lowest excited singlet discussed above, I approximate the relative energies of the excited singlet (S_1), S^+ and S^- charged species and the triplet state in the crystal by computing their ωB97X-D/6-31G* energies of clusters with seven chromophore molecules. Energy differences of S_0S_1, and S^+S^- and the two independent triplets (TT) with respect to S_0S_0 are shown in Table 3.

Computed energies for the charges species of Tc, DPT, and Rub appear rather high in energy with respect to S_0S_1 (and TT); hence, they should be ruled out as intermediate states in a two-step SF mechanism upon photoexcitation to the lowest optical states. These results are in agreement with previous computations of Tc.[59] The two independent triplets are ~0.1 eV above the excited singlet in Tc and are energetically favored in DPT and Rub.

Table 3. Energy Difference (in eV) of S_0S_1, S^+S^-, and TT (as two independent triplets) Diabatic States with Respect to S_0S_0 for Three Compounds Computed at the ωB97X-D/6-31G* Level

	Tc	DPT	Rub
S_0S_1	3.02	2.91	2.87
TT	3.16	2.75	2.46
S^+S^-	5.13	4.68	4.37

C. Simulation of Single and Multiexcitonic States in Dimers. The smallest necessary model to characterize the fission process in molecular materials must contain at least two coupled chromophores. Besides, contrary to the delocalized nature attributed to the optical state, a recent computational study[59] affirms that the multiexcitonic state of Tc localizes over a molecular pair. Therefore, I will take nearest neighbor pairs of Tc, DPT, and Rub in the crystallographic direction with the largest electronic coupling (as discussed above) as the workhorse models to explore their SF mechanisms (Figure 7).

In addition, in order to analyze possible dependences of the chromophore coupling on the intermolecular orientation, I will compare the behavior a total of five first-neighbor dimers in DPT (Figure 8), corresponding to two slip-stacked conformations and three pairs where the tetracene units are laterally disposed. Among them, the staggered dimer is the one with the shortest intermolecular distance (Figure 7).

Qualitatively, the electronic structure of the low-lying states of any of these molecular pairs can be obtained as different electronic occupations of the monomers' HOMOs and LUMOs. In a simplified four electrons in four orbitals model, the zero-order wave functions of the four lowest singlet states in a symmetric homodimer can be expressed as CSFs

$$|S_0\rangle = |S_0^0 S_0^0\rangle \tag{2}$$

$$|S_\pm\rangle = \frac{1}{\sqrt{2}}[|S_1^0 S_0^0\rangle \pm |S_0^0 S_1^0\rangle] \tag{3}$$

$$|TT\rangle = \frac{1}{\sqrt{3}}[|T_0 T_0\rangle + |T_+ T_-\rangle + |T_- T_+\rangle] \tag{4}$$

where S_0^0, S_1^0 are the ground and singly excited singlets, and T_0, T_+, and T_- are the three M_S triplet microstates of the monomer. The energies of these states up to first order in the intermolecular interaction are

$$E_0 = 2\varepsilon_0 + W_0;\ W_0 = 4J_{HH} - 2K_{HH} \tag{5}$$

$$E_\pm = \varepsilon_0 + \varepsilon_1 + W_1 \pm \beta;\ W_1 = \frac{W_0}{2} + 2J_{HL} - K_{HL} \tag{6}$$

$$E_{TT} = 2\varepsilon_T + W_{TT};$$
$$W_{TT} = J_{HH} - K_{HH} + 2(J_{HL} - K_{HL}) + J_{LL} - K_{LL} \tag{7}$$

where ε_i are the energies of the monomer states, W_I are Coulombic interaction energies for each state, H and L labels refer to the HOMO and LUMO of the monomer, and J and K are the Coulomb and exchange integrals between orbitals of different monomers in the dimer. The β parameter is a measure of the energy splitting between the two singly excited states, and in the considered model, takes the form of eq 8

$$\beta = 2(h_A l_A | h_B l_B) - (h_A h_B | l_A l_B) \tag{8}$$

where the round brackets indicate spatial two-electron integral between the HOMO, h_A and h_B, and LUMO, l_A and l_B, of the two chromophores.

Transition moments to the $S_\pm$ states can be approximated as linear combinations of the monomer moments (eq 9), which anticipate S_+ as the bright state for homodimers with parallel transition moments. Other intermolecular orientations will result in intermediate situations. In addition, the energy

dx.doi.org/10.1021/ct4007635 | J. Chem. Theory Comput. XXXX, XXX, XXX−XXX

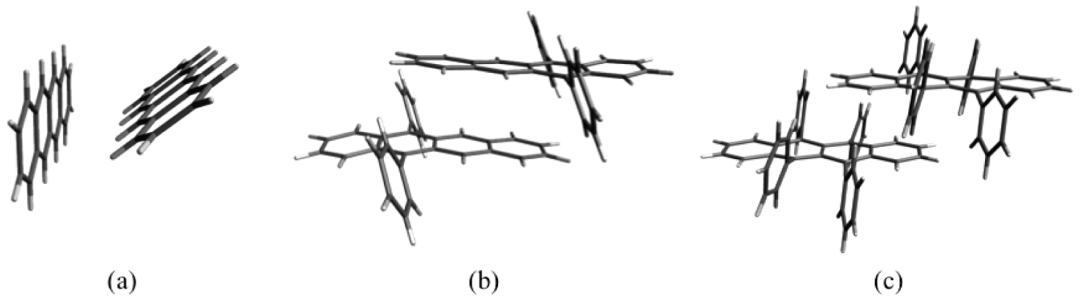

Figure 7. Nearest neighbor molecular dimers of (a) Tc, (b) DPT, and (c) Rub.

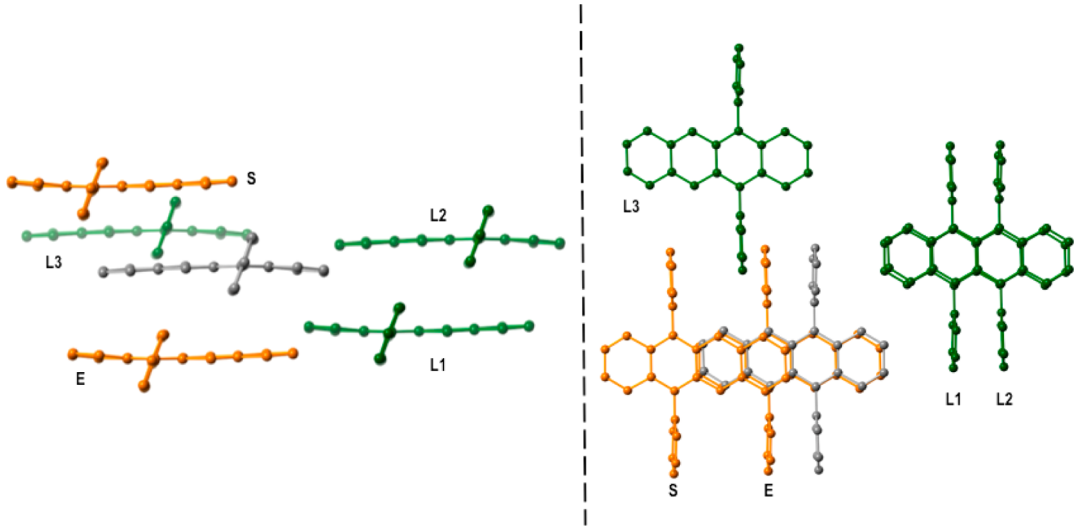

Figure 8. Two perpendicular views of the five first-neighbor dimers in DPT. Orange and green frames indicate slip-stack, i.e., eclipsed (E), staggered (S), and lateral (L1, L2, and L3) conformations, with respect to the gray reference molecule.

ordering between $S_{\pm}$ depends on the relative disposition between the monomer transition moments, i.e., $E_+ > E_-$ (parallel) and $E_- > E_+$ (linear).[60]

$$\mu_{\pm} = \frac{1}{\sqrt{2}}(\boldsymbol{\mu}_{\mathbf{A}} \pm \boldsymbol{\mu}_{\mathbf{B}}) \tag{9}$$

Now, moving to ab initio calculations within the RASCI framework while keeping the simple four electrons in four orbitals model in mind, it seems rather natural to take the four singly occupied orbitals from ROHF quintet wave functions as the RAS2 subspace in RAS(4,4)-2SF computation of the low-lying states of the Tc, DPT, and Rub dimers. Commonly, these orbitals are obtained as the in phase and out of phase combinations of the two HOMOs and two LUMOs, respectively, and delocalize over the two molecular moieties.[61] As a consequence, they are not the most appealing single electron functions in order to analyze the long-lying states by means of the four electrons in four orbitals model described above, that is, excitations within a monomer. Providentially, the orbital invariance within the RAS2 subspace allows performing orbital rotations toward fragment-localized orbitals (≥99.98% Mulliken charges on one of the two molecules) as orthogonal linear combinations between the reference canonical orbitals (Figure 9). The use of the fragment orbitals gives a direct and simple picture for the interpretation of the diagonalized states, and neutral and CT like type of excitations are immediately identified. In spite of the warnings given by Krylov and co-workers,[25] there were no convergence issues during the RAS-SF calculations using fragment orbitals.

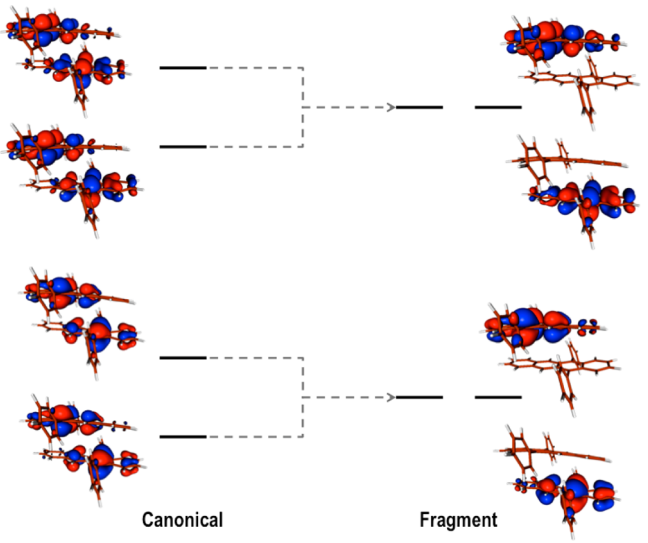

Figure 9. Fragment-localized orbitals (right) as linear combinations of the ROHF canonical orbitals (left) for the DPT eclipsed dimer.

The main contributions to the low-lying computed states are shown in Table 4. The RAS-2SF diagonalized wave functions of the four singlets corresponding to the CSFs in eqs 2−4 are mostly composed by electronic configurations within the RAS2 space, especially the ground ($\mathbf{S_0}$) and the doubly excited dark ($\mathbf{D}$) states (Table 3). The two singly excited singlets present larger roles of RAS1-to-RAS2 and RAS2-to-RAS3 electronic

dx.doi.org/10.1021/ct4007635 | J. Chem. Theory Comput. XXXX, XXX, XXX−XXX

Table 4. Contributions (in %) to the Electronic Wavefunctions of S_0, S_+, S_-, and D States of Tc, DPT, and Rub Nearest Neighbour Dimers

S_0	$h_A^2h_B^2$	$h_A^2l_B^2$	$l_A^2h_B^2$	RAS2
Tc	84.1	4.5	4.3	93.2
DPT	82.7	5.1	5.1	93.1
Rub	82.5	5.2	5.2	93.2
S_+	$h_A^1l_A^1h_B^2$	$h_A^2h_B^1l_B^1$		RAS2
Tc	50.4	3.8		79.5
DPT	28.7	28.8		76.7
Rub	34.1	34.1		76.3
S_-	$h_A^1l_A^1h_B^2$	$h_A^2h_B^1l_B^1$		RAS2
Tc	17.0	41.5		78.8
DPT	35.8	35.7		76.4
Rub	35.5	35.4		76.1
D		$h_A^1l_A^1h_B^1l_B^1$		RAS2
Tc		96.5		99.6
DPT		99.3		99.9
Rub		99.8		100.0

promotions (10−14%). This is a qualitative indication of the different impact that the lack of dynamical correlation will have in the excitation energies of $\mathbf{S}_\pm$ and **D**, as it has been previously observed in similar calculations.[55] In other words, double excitations outside RAS2 are expected to have larger impacts in $\mathbf{S}_\pm$ than in $\mathbf{S}_0$ or **D**; hence, RAS-2SF is anticipated to overestimate transition energies to $\mathbf{S}_\pm$ compared to **D**.

The full electronic occupation of the molecular HOMOs constitutes the main configuration in the ground state wave function, with considerable participation of neutral closed shell double excitations to the LUMOs. HOMO-to-LUMO promotions within a monomer are the major contributions to the $\mathbf{S}_\pm$ states (eq 3). The **D** state is almost entirely obtained as spin adapted combination of four unpaired electrons configurations. In the Tc dimer, the two molecules are not equivalent, which is reflected by the asymmetric contributions of excitation on either monomer. On the other hand, there are no distinction between *A*/*B* monomers in DPT and Rub resulting in symmetric amplitudes in all states.

As shown in Table 5, the energy ordering of $\mathbf{S}_+$ and $\mathbf{S}_-$ and the related oscillator strengths in DPT and Rub dimers are well in agreement with the relative orientation of the transition dipole moments of the monomers discussed above, i.e., parallel moments in all cases except for the L3 dimer of DPT (antiparallel). Oscillator strengths are of similar order in all cases, with larger transition probabilities in the lateral DPT dimers compared to the two slip-stacked conformers. The Tc dimer represents a mix situation between parallel and linear relative orientations, with transition to the two singly excited states partially allowed.

Table 5. Energy Gap ($\Delta E(\pm)$, in kcal/mol), Oscillator Strengths, and Charge Transfer Nature for S_+ and S_- States of all Tc, DPT, and Rub Studied Dimers

		osc. str.		% CT		
	$\Delta E(\pm)$	S_+	S_-	S_+	S_-	D
Tc	2.91	0.411	0.174	21.2	16.0	3.0
DPT						
eclipsed	−4.96	0.776	0.000	15.1	0.1	0.2
staggered	−0.36	0.772	0.000	14.7	0.1	0.6
lateral 1	−0.51	0.975	0.000	0.0	0.0	0.0
lateral 2	−0.37	0.979	0.000	0.1	0.1	0.3
lateral 3	1.20	0.978	0.006	0.0	0.0	0.0
Rub	−0.94	0.924	0.000	2.7	0.1	0.1

$\Delta E(\pm) = E(S_-) - E(S_+)$.

The presence of CT configurations in the computed states informs about the ionic nature of the wave function, but it does not necessarily imply a true electronic transfer between monomers. In fact, only the $\mathbf{S}_\pm$ states of Tc show sizable real CT, with 0.18 ($\mathbf{S}_+$) and 0.16 ($\mathbf{S}_-$) displaced electrons. The $\mathbf{S}_+$ states of eclipsed and staggered DPT dimers have large weights of CT configurations, but overall there is no neat electron transfer. Similar situation is obtained for the Rub dimer but with a much lower CT contribution (2.7%). The DPT lateral dimers show no CT character in any of the studied states. It is worth mentioning that although the **D** state is almost entirely constituted by the *TT* configuration (eq 4) it contains some nonzero CT contributions, accounting for 3.0%, 0.2%, 0.6%, and 0.1% of the wave function in Tc, DPT (eclipsed and staggered), and Rub, respectively.

C.1. Chromophore Coupling. The type and strength of electronic coupling between chromophores is a crucial property for the efficiency of the SF process and controls the rate of the conversion of the optical state to the dark state.[57,62−64] The SF possible mechanisms are classified depending on the nature of the interaction between these two states as direct, mediated (through CT states), or by as a two-step process with the presence of real CT intermediates.[22] By virtue of the energy differences in Table 3, the two-step mechanism will no longer be taken into consideration here. In order to explore the couplings in the Tc, DPT, and Rub dimers, I take the 20 spin-adapted singlet states that can be constructed with four electrons in four orbitals as the diabatic states. The detailed description of these states can be found as part of the Supporting Information. The diabatic basis allows decomposing the coupling between initial and final states in first- and second-order contributions (first and second terms in eq 10), which can be related to the strength of direct and mediated interactions.[23]

$$\langle S_0^0S_1^0|H|TT\rangle - \sum_{X\neq TT,S_0^0S_1^0} \frac{\langle S_0^0S_1^0|H|X\rangle\langle X|H|TT\rangle}{\Delta E_X} \quad (10)$$

The computed direct and indirect couplings lie within the energy range obtained with multistate density functional results for Tc.[64] The computed direct couplings of *TT* to the states with a singly excited monomer are of the order of up to few meV (Table 6). As shown in Figure 10, the largest couplings of *TT* are obtained for the CT states (up to ∼200 meV). Because

Table 6. First- and Second-Order Couplings (in meV) between $S_0^0S_1^0$ and *TT* Diabats[a]

dimer	1st	2nd	total
Tc	−2.2	−52.1	−54.3
DPT			
eclipsed	0.3	3.7	3.9
staggered	0.2	−1.0	−0.8
Rub	0.0	0.0	0.0

[a]The total values correspond to the addition of the two contributions as described in eq 10. Diabatic energies computed with ωB97X-D (ΔE_X denominator of eq 10). CT states have been obtained within the CDFT.

dx.doi.org/10.1021/ct4007635 | J. Chem. Theory Comput. XXXX, XXX, XXX−XXX

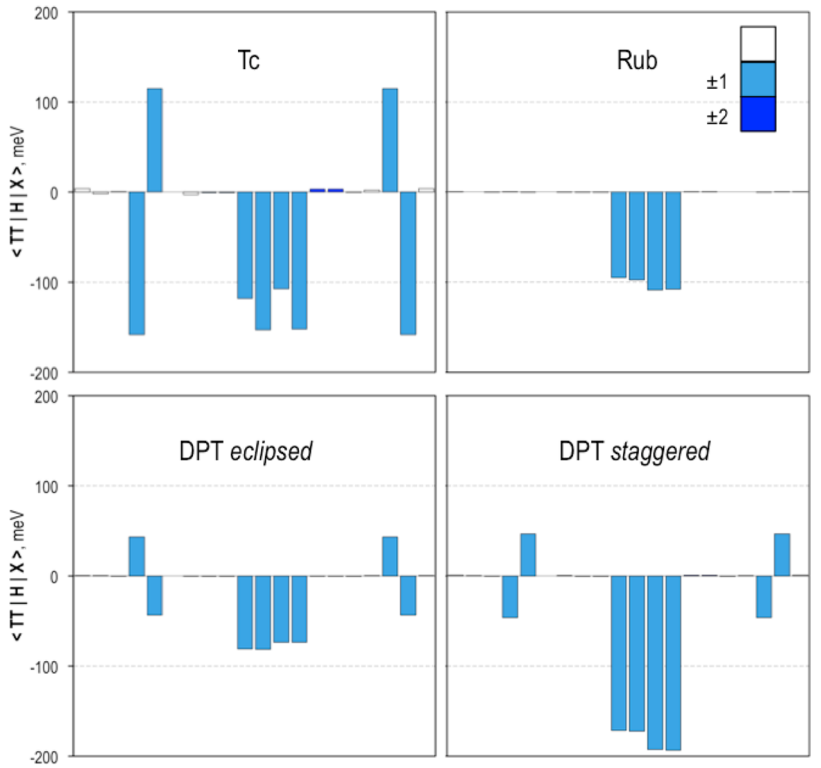

Figure 10. Direct couplings (in meV) of *TT* with the rest of diabatic singlets. Light and deep blue refer to ± and +2/−2 CT states. The complete set of couplings between diabatic states can be found in the Supporting Information.

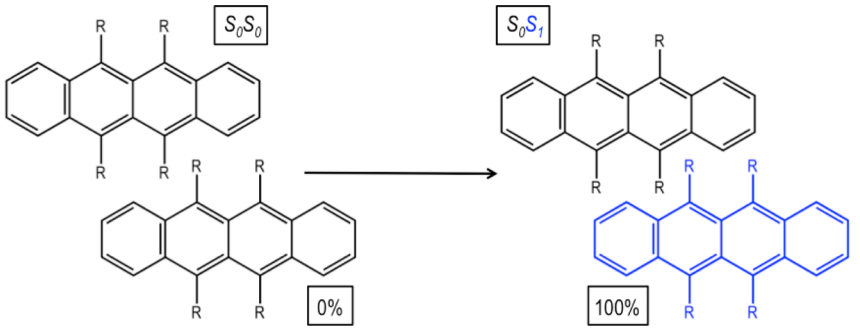

Figure 11. Schematic description of the intramolecular distortion model from S_0S_0 to S_0S_1.

of the energy difference denominator in the second-order term ($\Delta E_X = 2E_X - E_{TT} - E_{S_0^0S_1^0}$),[61] the largely dominant contributions to the mediated interaction come from the two lowest CT diabats ($S_0^-S_0^+$ and $S_0^+S_0^-$). Their matrix elements with *TT* have similar magnitudes but with different signs, while the coupling of these CT states to $S_0^0S_1^0$ have close values and the same sign, resulting in an important cancelation in the mediated term. Similar reasoning can be made for the energetically much higher $S_1^-S_1^+$ and $S_1^-S_1^+$ states, although their role in the interaction is basically insignificant. These issues have been recently discussed in detail by Jovanovic and collaborators[65] and suggest that in order to increase the coupling strength it would be desirable to break the symmetry of the dimer, thus breaking the balance between the ∓ and ± contributions.

The comparison between the different dimers indicates that the magnitude of the direct and mediated interactions decreases along the series Tc > DPT-*ecl* > DPT-*stag* > Rub (Table 6). This behavior is directly linked to the amount of CT contributions present in the multiexcitonic and optical adiabatic states found for these dimers as discussed above (Table 5). Overall, these results indicate an intermediate situation between direct and mediated SF mechanism in Tc, while in DPT the interchromophoric coupling is dominated by mediated interactions through cation/anion states. In Rub, the first- and second-order contributions are of similar magnitude but smaller than the two slip-stacked pairs in DPT.

Also, it is worth mentioning that the trend in the magnitude of the coupling in Table 6 is in agreement with the average molecular interaction strength (*A* in eq 1) obtained at the DFT level and discussed previously.

C.2. SF Assisted by Intramolecular Motion. Pulse-induced transient absorption measurements on tetracene[66] have shown that SF might be assisted by intermolecular motion based on low frequency vibrational modes. Excitation of such lattice vibrations has a direct impact on the coupling between the single and multiplexciton states, facilitating the transfer between them. In pentacene and tetracene, it has been argued that these breathing-like distortions tune the interchromophore coupling

dx.doi.org/10.1021/ct4007635 | J. Chem. Theory Comput. XXXX, XXX, XXX−XXX

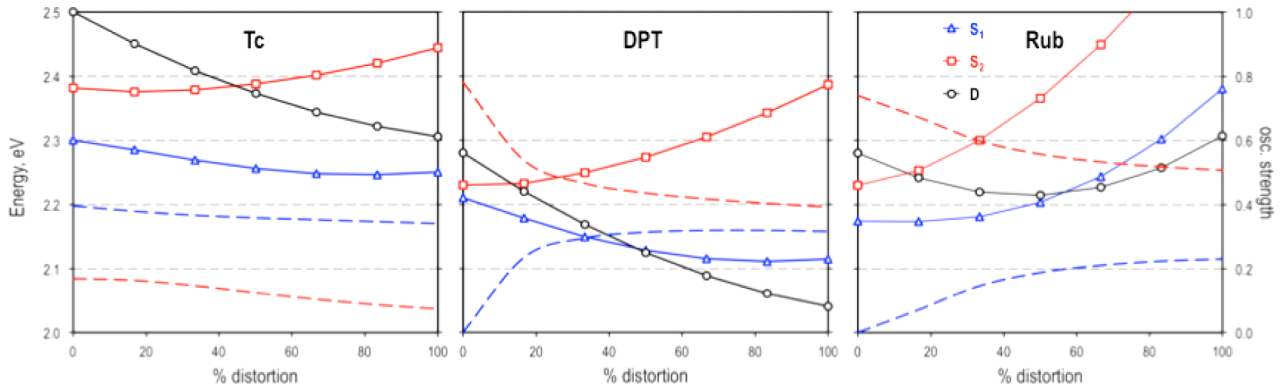

Figure 12. RAS potential energy profiles (in eV) along the S_0S_0 to S_0S_1 coordinate for Tc, DPT, and Rub nearest neighbor dimers. Blue and red dashed lines correspond to the transition oscillator strengths to $\mathbf{S_1}$ and $\mathbf{S_2}$, respectively (secondary vertical axis).

by modifying the $\pi-\pi$ interactions between neighbor molecules.[55] Alternatively, intermolecular coupling could be tuned by shifting the relative energy levels of the monomers. In this sense, I propose here that intramolecular distortions might also act as alternative mediators in SF of Tc and its derivatives, in line with a recent study of Broer and collaborators, where SF was explored at the optimized geometry of the lowest singly excited state in 2-methyl-1,5-hexadiene as a model.[59]

As a qualitative model, I consider the molecular motion corresponding to the linear transit distortion between the ground state dimer (two molecules in the S_0 optimized geometry) and the dimer with one of the molecules at the lowest excited state geometry (Figure 11). This distortion basically corresponds to the backbone high frequency vibrational mode on one of the chromophores observed in the vibronic progression in the absorption and emission spectra discussed above. The intermolecular disposition between the monomers and the orientation angles of the substitution phenyls in DPT and Rub dimers have been fixed to the crystal parameters. The energies of $\mathbf{S_+}$ and **D** states are homogenously shifted to the experimental values at the ground state geometries, which basically accounts for the lack of dynamical correlation in RASCI[41] and the effects of the crystal environment. Given the intramolecular nature of the described distortion, it seems plausible to consider that both effects, i.e., the crystal environment surrounding of the dimers and the lack of dynamic correlation, will remain constant along the path.

Potential energy plots of DPT and Rub excited states in Figure 12 suggest that after fast decay of the optical $\mathbf{S_2}$ state to the lowest $\mathbf{S_1}$ (Kasha's rule) the system goes through geometry relaxation on the $\mathbf{S_1}$ surface. Along this path, the dark state experiences faster energy stabilization than $\mathbf{S_1}$, eventually resulting in an energy degeneration of these two states, and potentially favoring the $\mathbf{S_1}$-to-**D** nonadiatic transition. This behavior is in agreement with ultrafast transient absorption and time-resolved emission experiments on DPT[31] and Rub,[33] indicating exergonic SF.

Although the dark state in Tc also stabilizes faster than $\mathbf{S_1}$ along the studied nuclear motion, the larger initial energy gap between $\mathbf{S_1}$ and **D** at the ground state geometry (0.20 eV) compared to DPT and Rub energy separations, prevents reaching a crossing point, with a shrunk energy gap at the S_0S_1 geometry of 0.05 eV, in good agreement with experimental measurements[22,27,48,67] and theoretical calculations[55,68] indicating the multiexciton state lying slightly above the optical state.

Finally, the computation of oscillator strengths to $\mathbf{S_1}$ and $\mathbf{S_2}$ (dashed lines in Figure 12) allows monitoring the mixing of their S_+/S_- character along the path (eq 3).

CONCLUSIONS

Computed absorption, emission, and adiabatic transition energies to the bright state of Tc, DPT, and Rub in solution are in excellent agreement with experimental values. Computed relative energies between planar and twisted forms of Rub and comparison of TDDFT transition energies to experimental spectra confirm that the nonplanar form is preferred in solution. The electronic structure characterization of molecular species in solution has been used as a background for the afterward analysis of the electronic structure properties of Tc, DPT, and Rub in their extended structures by means of cluster calculations.

Computational and spectroscopic experimental evidence suggest that while tetracene and the two studied derivatives have very similar electronic structure, their different chemical substitution results in distinct crystal packaging, producing different interchromophore interactions. The delocalization of the initially excited state has been indirectly measured to extend at least seven molecules. In all three cases, the diabatic CT state lies rather high in energy with respect to the lowest single exciton, which rules out the possibility of a two-step SF mechanism. Electronic structure calculations of molecular dimers indicate that CT configurations play a much deeper role in Tc compared to DPT and Rub. As a result, the computed first- and second-order couplings between the bright and dark state are larger in the nonsubstituted case.

Finally, I have discussed the possibility of SF process assisted by an intramolecular motion. The model considered qualitatively corresponds to the high-frequency C−C backbone breathing responsible of the vibronic coupling observed in absorption and emission spectra. The computed potential energy profiles for the low-lying states of Tc, DPT, and Rub are in agreement with previous statements based on experimental measurements and identify the distortion as a plausible catalyst for SF in the extended structures. This distortion model is of special interest in DPT and Rub, where the intermolecular vibrations are supposed to be largely suppressed by the substitution of the tetracene moiety.

dx.doi.org/10.1021/ct4007635 | J. Chem. Theory Comput. XXXX, XXX, XXX−XXX

■ ASSOCIATED CONTENT

Supporting Information

Symmetric CC stretching bond frequencies in solution; vertical absorption, emission and adiabatic excitation energies in solution; transition energies to the lowest excited singlet for molecular clusters with up to 13 molecules; graphical representation of the molecular clusters; nomenclature for the neutral and ionic monomer states; and spin-adapted diabatic singlet states as combination of monomer states. This material is available free of charge via the Internet at http://pubs.acs.org.

■ AUTHOR INFORMATION

Corresponding Author

*E-mail: david.casanova@ehu.es.

Notes

The authors declare no competing financial interest.

■ ACKNOWLEDGMENTS

Financial support for this work was provided by the Spanish Ministerio de Ciencia e Innovación through project 2011-23862-C02-02/BQU and the Generalitat de Catalunya through project 2009SGR-1459. The author gratefully acknowledges the Ramón y Cajal program (RyC 2008-0223) and the IKERBASQUE, Basque Foundation for Science for financial support.

■ REFERENCES

(1) Singh, S.; Jones, W. J.; Siebrand, W.; Stoicheff, B. P.; Schneider, W. G. *J. Chem. Phys.* **1965**, *42*, 330.
(2) Geacintov, N.; Pope, M.; Vogel, F. *Phys. Rev. Lett.* **1969**, *22*, 593.
(3) Groff, R. P.; Avakian, P.; Merrifield, R. E. *Phys. Rev. B* **1970**, *1*, 815.
(4) Chan, W.-L.; Tritsch, J. R.; Zhu, X. Y. *J. Am. Chem. Soc.* **2012**, *134*, 18295.
(5) Burdett, J. J.; Bardeen, C. J. *Acc. Chem. Res.* **2013**, *46*, 1312.
(6) Burgos, J.; Pope, M.; Swenberg, C. E.; Alfano, R. R. *Phys. Status Solidi B* **1977**, *83*, 249.
(7) Jundt, C.; Klein, G.; Sipp, B.; Le Moigne, J.; Joucla, M.; Villaeys, A. A. *Chem. Phys. Lett.* **1995**, *241*, 84.
(8) Chan, W.-L.; Ligges, M.; Jailaubekov, A.; Kaake, L.; Miaja-Avila, L.; Zhu, X.-Y. *Science* **2011**, *334*, 1541.
(9) Wilson, M. W. B.; Rao, A.; Ehrler, B.; Friend, R. H. *Acc. Chem. Res.* **2013**, *46*, 1330.
(10) Lee, J.; Bruzek, M. J.; Thompson, N. J.; Sfeir, M. Y.; Anthony, J. E.; Baldo, M. A. *Adv. Mater.* **2013**, *25*, 1445.
(11) Rademaker, H.; Hoff, A. J.; Van Grondelle, R.; Duysens, L. N. M. *Biochim. Biophys. Acta, Bioenerg.* **1980**, *592*, 240.
(12) Austin, R. H.; Baker, G. L.; Etemad, S.; Thompson, R. *J. Chem. Phys.* **1989**, *90*, 6642.
(13) Nozik, A. J.; Ellingson, R. J.; Mićić, O. I.; Blackburn, J. L.; Yu, P.; Murphy, J. E.; Beard, M. C.; Rumbles, G. In Twenty-Seventh DOE Solar Photochemistry Research Conference, Warrenton, Virginia, 2004, p 63.
(14) Lee, J.; Jadhav, P.; Reusswig, P. D.; Yost, S. R.; Thompson, N. J.; Congreve, D. N.; Hontz, E.; Van Voorhis, T.; Baldo, M. A. *Acc. Chem. Res.* **2013**, *46*, 1300.
(15) Jadhav, P. J.; Mohanty, A.; Sussman, J.; Lee, J.; Baldo, M. A. *Nano Lett.* **2011**, *11*, 1495.
(16) Jadhav, P. J.; Brown, P. R.; Thompson, N.; Wunsch, B.; Mohanty, A.; Yost, S. R.; Hontz, E.; Van Voorhis, T.; Bawendi, M. G.; Bulović, V.; Baldo, M. A. *Adv. Mater.* **2012**, *24*, 6169.
(17) Reusswig, P. D.; Congreve, D. N.; Thompson, N. J.; Baldo, M. A. *Appl. Phys. Lett.* **2012**, *101*, 113304.
(18) Congreve, D. N.; Lee, J.; Thompson, N. J.; Hontz, E.; Yost, S. R.; Reusswig, P. D.; Bahlke, M. E.; Reineke, S.; Van Voorhis, T.; Baldo, M. A. *Science* **2013**, *340*, 334.
(19) Ehrler, B.; Walker, B. J.; Böhm, M. L.; Wilson, M. W. B.; Vaynzof, Y.; Friend, R. H.; Greenham, N. C. *Nat. Commun.* **2012**, *3*, 1019.
(20) Shockley, W.; Queisser, H. J. *J. Appl. Phys.* **1961**, *32*, 510.
(21) Paci, I.; Johnson, J. C.; Chen, X.; Rana, G.; Popovifá, D. k.; David, D. E.; Nozik, A. J.; Ratner, M. A.; Michl, J. *J. Am. Chem. Soc.* **2006**, *128*, 16546.
(22) Smith, M. B.; Michl, J. *Chem. Rev.* **2010**, *110*, 6891.
(23) Smith, M. B.; Michl, J. *Annu. Rev. Phys. Chem.* **2013**, *64*, 361.
(24) Zimmerman, P. M.; Musgrave, C. B.; Head-Gordon, M. *Acc. Chem. Res.* **2013**, *46*, 1339.
(25) Feng, X.; Luzanov, A. V.; Krylov, A. I. *J. Phys. Chem. Lett.* **2013**, *4*, 3845.
(26) Lee, J.; Jadhav, P.; Baldo, M. A. *Appl. Phys. Lett.* **2009**, *95*, 033301.
(27) Burdett, J. J.; Muller, A. M.; Gosztola, D.; Bardeen, C. J. *J. Chem. Phys.* **2010**, *133*, 144506.
(28) Rao, A.; Wilson, M. W. B.; Hodgkiss, J. M.; Albert-Seifried, S.; Bässler, H.; Friend, R. H. *J. Am. Chem. Soc.* **2010**, *132*, 12698.
(29) Wang, C.; Tauber, M. J. *J. Am. Chem. Soc.* **2010**, *132*, 13988.
(30) Johnson, J. C.; Nozik, A. J.; Michl, J. *J. Am. Chem. Soc.* **2010**, *132*, 16302.
(31) Roberts, S. T.; McAnally, R. E.; Mastron, J. N.; Webber, D. H.; Whited, M. T.; Brutchey, R. L.; Thompson, M. E.; Bradforth, S. E. *J. Am. Chem. Soc.* **2012**, *134*, 6388.
(32) Najafov, H.; Lee, B.; Zhou, Q.; Feldman, L. C.; Podzorov, V. *Nat. Mater.* **2010**, *9*, 938.
(33) Ryasnyanskiy, A.; Biaggio, I. *Phys. Rev. B* **2011**, *84*, 193203.
(34) Ma, L.; Zhang, K.; Kloc, C.; Sun, H.; Michel-Beyerle, M. E.; Gurzadyan, G. G. *Phys. Chem. Chem. Phys.* **2012**, *14*, 8307.
(35) Piland, G. B.; Burdett, J. J.; Kurunthu, D.; Bardeen, C. J. *J. Phys. Chem. C* **2013**, *117*, 1224.
(36) Marenich, A. V.; Olson, R. M.; Kelly, C. P.; Cramer, C. J.; Truhlar, D. G. *J. Chem. Theory Comput.* **2007**, *3*, 2011.
(37) Runge, E.; Gross, E. K. U. *Phys. Rev. Lett.* **1984**, *52*, 997.
(38) Casida, M. E. *Recent Advances in Density Function*; World Scientific: Singapore, 1995; Vol. *1*.
(39) Chai, J.-D.; Head-Gordon, M. *Phys. Chem. Chem. Phys.* **2008**, *10*, 6615.
(40) Stevens, W. J.; Basch, H.; Krauss, M. *J. Chem. Phys.* **1984**, *81*, 6026.
(41) Casanova, D.; Head-Gordon, M. *Phys. Chem. Chem. Phys.* **2009**, *11*, 9779.
(42) Casanova, D. *J. Chem. Phys.* **2012**, *137*, 084105.
(43) Casanova, D. *J. Comput. Chem.* **2013**, *34*, 720.
(44) Wu, Q.; Van Voorhis, T. *Phys. Rev. A* **2005**, *72*, 024502.
(45) Shao, Y.; Molnar, L. F.; Jung, Y.; Kussmann, J.; Ochsenfeld, C.; Brown, S. T.; Gilbert, A. T. B.; Slipchenko, L. V.; Levchenko, S. V.; O'Neill, D. P.; DiStasio, R. A., Jr; Lochan, R. C.; Wang, T.; Beran, G. J. O.; Besley, N. A.; Herbert, J. M.; Lin, C. Y.; Voorhis, T. V.; Chien, S. H.; Sodt, A.; Steele, R. P.; Rassolov, V. A.; Maslen, P. E.; Korambath, P. P.; Adamson, R. D.; Austin, B.; Baker, J.; Byrd, E. F. C.; Dachsel, H.; Doerksen, R. J.; Dreuw, A.; Dunietz, B. D.; Dutoi, A. D.; Furlani, T. R.; Gwaltney, S. R.; Heyden, A.; Hirata, S.; Hsu, C.-P.; Kedziora, G.; Khalliulin, R. Z.; Klunzinger, P.; Lee, A. M.; Lee, M. S.; Liang, W.; Lotan, I.; Nair, N.; Peters, B.; Proynov, E. I.; Pieniazek, P. A.; Rhee, Y. M.; Ritchie, J.; Rosta, E.; Sherrill, C. D.; Simmonett, A. C.; Subotnik, J. E.; Iii, H. L. W.; Zhang, W.; Bell, A. T.; Chakraborty, A. K. *Phys. Chem. Chem. Phys.* **2006**, *8*, 3172.
(46) Käfer, D.; Ruppel, L.; Witte, G.; Wöll, C. *Phys. Rev. Lett.* **2005**, *95*, 166602.
(47) Petrenko, T.; Krylova, O.; Neese, F.; Sokolowski, M. *New J. Phys.* **2009**, *11*, 015001.
(48) Tomkiewicz, Y.; Groff, R. P.; Avakian, P. *J. Chem. Phys.* **1971**, *54*, 4504.
(49) Robertson, J. M.; Sinclair, V. C.; Trotter, J. *Acta Crystallogr.* **1961**, *14*, 697.
(50) Holmes, D.; Kumaraswamy, S.; Matzger, A. J.; Vollhardt, K. P. C. *Chem.—Eur. J.* **1999**, *5*, 3399.

(51) Kitamura, C.; Matsumoto, C.; Kawatsuki, N.; Yoneda, A.; Kobayashi, T.; Naito, H. *Anal. Sci.: X-Ray Struct. Anal. Online* **2006**, *22*, x5.
(52) Jurchescu, O. D.; Meetsma, A.; Palstra, T. T. M. *Acta Cryst. B* **2006**, *62*, 330.
(53) Sundar, V. C.; Zaumseil, J.; Podzorov, V.; Menard, E.; Willett, R. L.; Someya, T.; Gershenson, M. E.; Rogers, J. A. *Science* **2004**, *303*, 1644.
(54) da Silva Filho, D. A.; Kim, E. G.; Brédas, J. L. *Adv. Mater.* **2005**, *17*, 1072.
(55) Zimmerman, P. M.; Bell, F.; Casanova, D.; Head-Gordon, M. *J. Am. Chem. Soc.* **2011**, *133*, 19944.
(56) Lim, S.-H.; Bjorklund, T. G.; Spano, F. C.; Bardeen, C. J. *Phys. Rev. Lett.* **2004**, *92*, 107402.
(57) Johnson, J. C.; Nozik, A. J.; Michl, J. *Acc. Chem. Res.* **2013**, *46*, 1290.
(58) Johnson, J. C.; Akdag, A.; Zamadar, M.; Chen, X.; Schwerin, A. F.; Paci, I.; Smith, M. B.; Havlas, Z.; Miller, J. R.; Ratner, M. A.; Nozik, A. J.; Michl, J. *J. Phys. Chem. B* **2013**, *117*, 4680.
(59) Havenith, R. W. A.; de Gier, H. D.; Broer, R. *Mol. Phys.* **2012**, *110*, 2445.
(60) Kasha, M. *Spectroscopy of the Excited State*; Plenum Press: New York, 1976.
(61) Energies of the charge transfer states have been obtained within the constrained DFT (CDFT) approach in conjuntion with the ωB97X-D functional.
(62) Greyson, E. C.; Vura-Weis, J.; Michl, J.; Ratner, M. A. *J. Phys. Chem. B* **2010**, *114*, 14168.
(63) Vallett, P. J.; Snyder, J. L.; Damrauer, N. H. *J. Phys. Chem. A* **2013**, *117*, 10824.
(64) Chan, W.-L.; Berkelbach, T. C.; Provorse, M. R.; Monahan, N. R.; Tritsch, J. R.; Hybertsen, M. S.; Reichman, D. R.; Gao, J.; Zhu, X. Y. *Acc. Chem. Res.* **2013**, *46*, 1321.
(65) Jovanovic, M.; Havlas, Z.; Michl, J. Unpublished results referenced in ref 12.
(66) Grumstrup, E. M.; Johnson, J. C.; Damrauer, N. H. *Phys. Rev. Lett.* **2010**, *105*, 257403.
(67) Chan, W.-L.; Ligges, M.; Zhu, X. Y. *Nat. Chem.* **2012**, *4*, 840.
(68) Zimmerman, P. M.; Zhang, Z.; Musgrave, C. B. *Nat. Chem.* **2010**, *2*, 648.